Dr. R. Nagarajan | Dr. Sankha Karmakar
Department of Chemical Engineering | IIT Madras

SAND IN AN HOURGLASS

Shrey Malik (CH22B004) | Ojas Phadake (CH22B007) | Aayush Bhakna (CH22B008)
Akanksh C J (CH22B010) | Shivansh Gupta (CH22B011) | Bharath Sajeev (CH22B012)
Om Mineeyar (CH22B014) | Deepanjhan Das (CH22B020)

Submitted on April 27, 2024

Abstract - In this work, we provide a critical analysis of the many scholarly articles and papers dealing with the flow of granular material inside an hourglass, using the concepts discussed in the course CH2015 - Fluid and Particle Mechanics.

1 Introduction

An hourglass is an instrument used to measure time by making use of granular materials like sand or ballotini, instead of liquids like oil or water. To study the mechanics involved in this device, we first need to properly describe its shape using appropriate assumptions.

After the shape has been defined, we go through other articles and papers to find models which would best describe the particle mechanics of granular flow in this system. We first look at the correlation proposed by Beverloo et al. (1961). Finding it unsatisfactory, we move on to a modified version of the same equation provided by Nedderman (1992, p.296) which better describes the mass flow rate $\dot{M}$ at the circular exit slot. This modified equation is also called the Rose-Tanaka-Beverloo-Nedderman (RTBN) correlation.

We then deal with the SWRG equation (Savage, 1965; Davidson and Nedderman, 1973) and the N equation (Nguyen, 1979), both of which assume that the Haar-Von Karman Hypothesis (Haar and Karman, 1909) is true. We analyse these equations with RTBN, and make conclusions on the basis of the comparison.

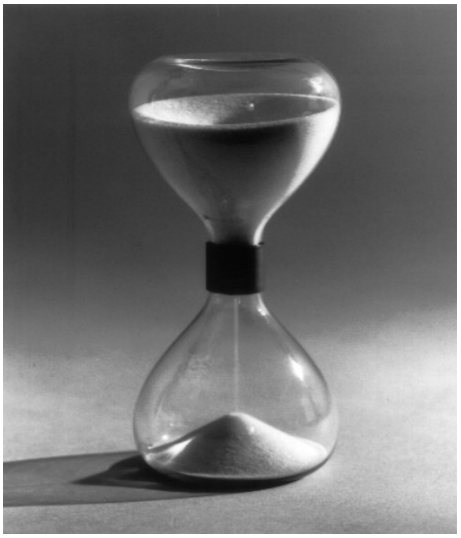

Figure 1: Traditional sandglass

Finally, we critically analyze other components of particle mechanics like radial stress, velocity field and density field provided in other reports or journals (Cleaver and Nedderman, 1993a; Hosseini-Ashrafi and Tuzun, 1993).

2 Important Concepts and Assumptions

2.1 *General Assumptions*

The following are the general conditions assumed throughout the different articles and papers we have used in this work:

- The shape of the hourglass is approximated to that of a frustum of some cone with head of the material at height H, width of the slot D and wall angle θ_w. This similarity between the shape of an hourglass and a conical hopper can be observed from their respective flow rate data (A A Mills, 1996, p.102-103).

- The material used in our work will be sand and sand-like materials (ballotini, granulated sugar, etc). These materials are assumed to be coarse ($d_p > 0.40$ mm) and have perfectly spherical particles (A A Mills, 1996, p.99).

- Some other assumptions include steady-incompressible flow, smooth walls (in case of RTBN and SWRG equations), radial gravity (in case of SWRG) and axisymmetric flow ($v_{\phi'} = 0$).

2.2 *Two-Dimensional Stress Tensor*

Considering a cartesian coordinate system, let AB denote the line of intersection of the X-Y plane and a plane P which is perpendicular to it. Then, the stress vector $\boldsymbol{t_n}$ exerted at some point on P is given by

$$\boldsymbol{t_n} = \boldsymbol{n} \cdot \boldsymbol{\sigma} \tag{2.2.1}$$

where $\boldsymbol{n}$ is the unit vector normal to AB and $\boldsymbol{\sigma}$ is the two-dimensional *stress tensor*.
Now, for no shear stresses to act on P, the stress vector $\boldsymbol{t_n}$ must have the same direction as $\boldsymbol{n}$. This means that $\boldsymbol{t_n} = a\boldsymbol{n}$ for some arbitrary constant a. As such, we can re-write the above equation as

$$\boldsymbol{\sigma} \cdot \boldsymbol{n} = a\boldsymbol{n} \tag{2.2.2}$$

This equation can be solved using the concept of eigenvalues and eigenvectors. The constant a will have two solutions given by the characteristic equation

$$a^2 - tr(\boldsymbol{\sigma})a + det(\boldsymbol{\sigma}) = 0 \tag{2.2.3}$$

These two eigenvalues are called the *principal stresses* and are denoted by σ_1 and σ_2. Putting the eigenvalues back into equation, we can find out the eigenvectors $\boldsymbol{n}_1$ and $\boldsymbol{n}_2$ corresponding to σ_1 and σ_2 respectively. These eigenvectors are called the *principal stress axes*.
Assuming that $\sigma_1 \geq \sigma_2$, we call σ_1 and σ_2 the *major* and *minor* principal stresses respectively. Now, let us change our perspective, and consider a cartesian coordinate system whose X'-Y' axes coincide with the principal stress axes $\boldsymbol{n}_1$ and $\boldsymbol{n}_2$. In this system, the stress tensor has a matrix representation of

$$\boldsymbol{\sigma} = \begin{pmatrix} \sigma_1 & 0 \\ 0 & \sigma_2 \end{pmatrix} \tag{2.2.4}$$

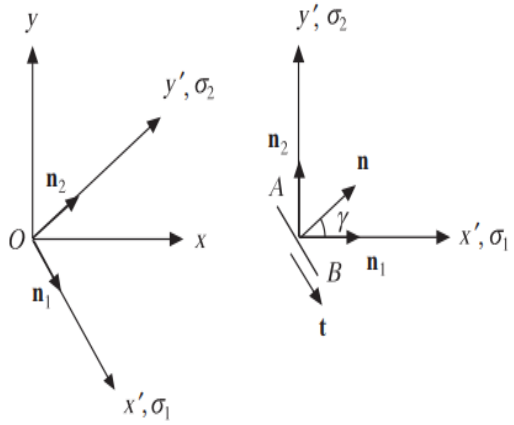

Figure 2: Figure describing the principal stress axes

Now, consider a plane which is perpendicular to the X'-Y' plane, such that its unit normal $\boldsymbol{n}$ is inclined at an angle γ measured anticlockwise from the $\boldsymbol{n}_1$ stress axes. Then, the formula for the normal stress N and the shear stress T can be written as

$$N \equiv \boldsymbol{t_n} \cdot \boldsymbol{n} = \sigma + \tau cos(2\gamma) \tag{2.2.5}$$

$$T \equiv \boldsymbol{t_n} \cdot \boldsymbol{t} = \tau sin(2\gamma) \tag{2.2.6}$$

where,

$$\sigma = \frac{\sigma_1 + \sigma_2}{2}; \quad \tau = \frac{\sigma_1 - \sigma_2}{2} \tag{2.2.7}$$

The *mean stress* σ is analogous to pressure in fluid mechanics, while the *deviator stress* τ represents the magnitude of the maximum shear stress. The variables σ, τ and γ are called the *Sokolovskii variables*, used extensively in analysis of granular statics (Sokolovskii, 1965).

2.3 *Rate of Deformation Tensor*

The rate of deformation tensor, also called *strain rate matrix*, is denoted by $\mathbf{C}$, where

$$\mathbf{C} \equiv -\frac{1}{2}(\nabla \mathbf{v} + (\nabla \mathbf{v})^T) \tag{2.3.1}$$

The diagonal components of $\mathbf{C}(C_{11}, C_{22}, C_{33})$ represent the rate of compression per unit length of line elements that are parallel to the coordinate axes. The off-diagonal elements of $\mathbf{C}(C_{12} = C_{21}, C_{13} = C_{31}, C_{23} = C_{32})$ are proportional to the rate at which the angle between two initially orthogonal line elements changes due to flow.
Another way to physically describe $\mathbf{C}$ would be to say that the diagonals components represent the instantaneous rate of change of *size*, while the off-diagonal components represent the instantaneous rate of change of *shape* of the corresponding system.

$$\mathbf{C} \cdot \boldsymbol{n} = a\boldsymbol{n} \tag{2.3.2}$$

We can use the eigenvector approach used in the previous subsection to define the *principal rates of deformation* c_1 and c_2 corresponding to the tensor $\mathbf{C}$. Now, let us consider a plane which is perpendicular to the X'-Y' plane, such that its unit normal $\boldsymbol{n}$ is inclined at an angle γ_* measured anticlockwise from the $\boldsymbol{n}_1$ stress axes. Then, the formula for C, which is the rate of compression in towards $\boldsymbol{n}$, and S, which is the rate of shear in direction of $\boldsymbol{t}$, can be written as

$$\begin{aligned} C &\equiv (\boldsymbol{n} \cdot \mathbf{C}) \cdot \boldsymbol{n} = c_* + s\ cos(2\gamma_*) \\ S &\equiv (\boldsymbol{n} \cdot \mathbf{C}) \cdot \boldsymbol{t} = s\ sin(2\gamma_*) \end{aligned} \tag{2.3.3}$$

where

$$c_* = \frac{c_1 + c_2}{2}; \quad s = \frac{c_1 - c_2}{2}, \quad c_1 \geq c_2 \tag{2.3.4}$$

2.4 *Equations for Plane Flow*

Let us consider a general constitutive equation which relates the rate of deformation tensor $\mathbf{C}$, the stress tensor $\boldsymbol{\sigma}$ and the solid fraction ν as

$$\mathbf{C} = \boldsymbol{A}(\boldsymbol{\sigma}, \nu) \tag{2.4.1}$$

This equation implies that the principal axes of the stress and rate of deformation tensors are aligned with each other, meaning $\gamma_* = \gamma$ (Hunter, 1983, p.136-137). This is called the *coaxiality condition*. Using this condition, we can rewrite equations of C and S as

$$\begin{aligned} C &= \mathbf{C}_{xx} = c_* + s\ cos(2\gamma) \\ S &= -\mathbf{C}_{xy} = s\ sin(2\gamma) \end{aligned} \tag{2.4.2}$$

Similarly,

$$\mathbf{C}_{yy} = c_* - s\ cos(2\gamma) \tag{2.4.3}$$

Using the above given equations, we can obtain a general relation describing the coaxiality condition as

$$sin2\gamma\ (\mathbf{C}_{xx} - \mathbf{C}_{yy}) + cos2\gamma\ (\mathbf{C}_{xy} + \mathbf{C}_{yx}) = 0 \tag{2.4.4}$$

Combining the general constitutive equation with the condition of rate independence and incompressibility allows us to form a new relation called *plastic potential flow rule* (Hunter, 1983, p.480-481). This new relation when combined with the above equations, give us a new general relation describing the flow rule as

$$sin\ \nu_d\ (\mathbf{C}_{xx} - \mathbf{C}_{yy}) + cos2\gamma\ (\mathbf{C}_{xy} + \mathbf{C}_{yx}) = 0 \tag{2.4.5}$$

where ν_d is the *angle of dilation*, defined as

$$sin\ \nu_d \ \equiv \ -\frac{c_1 + c_2}{c_1 - c_2} = -\frac{c_*}{s} \tag{2.4.6}$$

2.5 *Equations for Steady, Axisymmetric Flow*

For our convenience, we will be analysing the equations and concepts in spherical coordinate system with origin at the virtual apex of the conical hopper. Now, for axisymmetric flow, all variables depend only on r and θ, and the velocity field is given by

$$v_r = v_r(r, \theta); \quad v_\theta = v_\theta(r, \theta); \quad v_{\phi'} = 0 \tag{2.5.1}$$

Applying this to the components of the rate of deformation tensor $\mathbf{C}$, we get

$$\begin{aligned}\mathbf{C}_{r\phi'} &= \frac{-1}{2\ r\ sin\theta}\frac{\partial v_r}{\partial \phi'} = 0,\\ \mathbf{C}_{\theta\phi'} &= \frac{-1}{2\ r\ sin\theta}\frac{\partial v_\theta}{\partial \phi'} = 0,\\ \mathbf{C}_{\phi'\phi'} &= -\frac{(v_r + v_\theta \cot\theta)}{r}\end{aligned} \tag{2.5.2}$$

As $\mathbf{C}_{r\phi'} = 0$, $\mathbf{C}_{\theta\phi'} = 0$, and $\mathbf{C}_{\theta\phi'} \neq 0$ in general, the ϕ' direction coincides with a principal axis of $\mathbf{C}$. As mentioned before, $\mathbf{C}$ depends only on the stress tensor $\boldsymbol{\sigma}$ and the solid fraction ν. This means that the principal axis of $\boldsymbol{\sigma}$, say the σ_3 axis, coincides with the ϕ' direction as well. Also, as principal axes are mutually orthogonal, the σ_1 and σ_2 axes must lie in the r-θ plane.

The balance are equations are given as :
mass balance

$$\frac{\partial \rho}{\partial t} + \frac{1}{r^2}\frac{\partial(\rho r^2 \nu_r)}{\partial r} + \frac{1}{r\ sin\theta}\frac{\partial(\rho\ \nu_\theta\ sin\theta)}{\partial\theta} = 0 \tag{2.5.3}$$

momentum balance (r component)

$$\rho\left(\frac{\partial \nu_r}{\partial t} + \nu_r\frac{\partial \nu_r}{\partial r} + \frac{\nu_\theta}{r}\frac{\partial \nu_r}{\partial\theta} - \frac{\nu_\theta^2}{r}\right) + \frac{\partial \sigma_{rr}}{\partial r} + \frac{1}{r}\frac{\partial \sigma_{\theta r}}{\partial\theta} + \frac{2\sigma_{rr} - \sigma_{\theta\theta} - \theta_{\phi'\phi'} + \sigma_{r\theta}cot\theta}{r} + \rho g cos\theta = 0 \tag{2.5.4}$$

momentum balance (θ component)

$$\rho\left(\frac{\partial \nu_\theta}{\partial t} + \nu_r\frac{\partial \nu_\theta}{\partial r} + \frac{\nu_\theta}{r}\frac{\partial \nu_\theta}{\partial\theta} + \frac{\nu_r\nu_\theta}{r}\right) + \frac{\partial \sigma_{r\theta}}{\partial r} + \frac{1}{r}\frac{\partial \sigma_{\theta\theta}}{\partial\theta} + \frac{3\sigma_{r\theta} + (\sigma_{\theta\theta} - \sigma_{\phi'\phi'})cot\theta}{r} - \rho g sin\theta = 0 \tag{2.5.5}$$

These balance equations are not enough to describe the system on their own, and need to be supplemented by constitutive equations. The equations we will be using are the coaxiality condition and the flow rule. The equations when re-written in spherical coordinate form are as follows:

$$sin2\gamma'\left(\frac{1}{r}\frac{\partial v_\theta}{\partial\theta} + \frac{v_r}{r} - \frac{\partial v_r}{\partial r}\right) + cos2\gamma'\left(\frac{1}{r}\frac{\partial v_r}{\partial\theta} - \frac{v_\theta}{r} + \frac{\partial v_\theta}{\partial r}\right) = 0 \tag{2.5.6}$$

$$cos2\gamma'\left(\frac{1}{r}\frac{\partial v_\theta}{\partial\theta} + \frac{v_r}{r} + \frac{\partial v_r}{\partial r}\right) + sin\ \nu_d\left(\frac{1}{r}\frac{\partial v_\theta}{\partial\theta} + \frac{v_r}{r} - \frac{\partial v_r}{\partial r}\right) = 0 \tag{2.5.7}$$

where ν_d is the angle of dilation.
Finally, the stress components can be expressed in terms of mean stress and deviator stress as follows:

$$\begin{aligned}\boldsymbol{\sigma}_{\theta\theta} &= \sigma + \tau cos(2\gamma');\\ \boldsymbol{\sigma}_{r\theta} &= \boldsymbol{\sigma}_{\theta r} = -\tau sin(2\gamma');\\ \boldsymbol{\sigma}_{rr} &= \sigma - \tau cos(2\gamma')\end{aligned} \tag{2.5.8}$$

The axisymmetric flows, unlike the plane flow, has a significant problem that $\boldsymbol{\sigma}_{\phi'\phi'} \neq 0$. This makes it impossible for us to directly use the constitutive equations for plane flow without any additional assumptions. To counter this problem, we shall introdute a new assumption into our system, which would be the Haar-Von Karman Hypothesis.

2.6 *Brennen-Pearce Solution*

The governing equations for the case of a conical hopper having rough walls and vertical gravity can be written in dimensionless form as:

$$\frac{1}{\xi}\frac{\partial(\xi u)}{\partial\xi} + \frac{1}{\xi}\frac{\partial v}{\partial\theta} = 0 \tag{2.6.1}$$

$$u\frac{\partial u}{\partial\xi} + \frac{v}{\xi}\frac{\partial u}{\partial\theta} - \frac{v^2}{\xi} + \frac{\partial}{\partial\xi}[\bar{\sigma}(1 - \sin\phi\cos 2\gamma')] - \frac{1}{\xi}\frac{\partial}{\partial\theta}(\bar{\sigma}\sin\phi\sin 2\gamma') - \frac{2\bar{\sigma}\sin\phi\cos 2\gamma'}{\xi} + \cos\theta = 0 \tag{2.6.2}$$

$$u\frac{\partial v}{\partial \xi}+\frac{v}{\xi}\frac{\partial v}{\partial \theta}+\frac{uv}{\xi}- \frac{\partial}{\partial \xi}(\bar{\sigma}\sin\phi\sin 2\gamma')+\frac{1}{\xi}\frac{\partial}{\partial\theta}[\bar{\sigma}(1+\sin\phi\cos 2\gamma')]- \frac{2\bar{\sigma}\sin\phi\sin 2\gamma'}{\xi}-\sin\theta=0 \tag{2.6.3}$$

$$\sin 2\gamma'\left(\frac{\partial u}{\partial \xi}-\frac{1}{\xi}\frac{\partial v}{\partial\theta}-\frac{u}{\xi}\right) -\cos 2\gamma'\left(\frac{\partial v}{\partial\xi}+\frac{1}{\xi}\frac{\partial u}{\partial\theta}-\frac{v}{\xi}\right)=0 \tag{2.6.4}$$

These equations constitute a system of four first-order partial differential equations, and hence four boundary conditions must be specified in the ξ and θ directions.

Considering symmetric solutions, the normal component of velocity and the shear stress must vanish along the centerline $\theta = 0$. Hence

$$v(\xi,\theta=0)=0;\quad \gamma'(\xi,\theta=0)=0 \tag{2.6.5}$$

Along the wall, the normal component of velocity must vanish. Assuming that the friction boundary condition is valid, the wall boundary conditions are given by

$$v(\xi,\theta=\theta_w)=0;\quad \gamma'(\xi,\theta=\theta_w)=\gamma_w \tag{2.6.6}$$

Additional boundary conditions must be prescribed in the ξ direction. As in the case of the smooth wall, radial gravity problem, it is assumed that the material in the hopper is bounded from above and below by two traction-free surfaces T_1 and T_e (Figure 3). Thus along T_1 and T_e

$$\bar{\sigma}=0 \tag{2.6.7}$$

In 1978, Brennen and Pearce constructed an approximate solution using expansion in powers of θ where γ' and v are odd functions of θ whereas $\bar{\sigma}$ and u are even functions. A series solution can be constructed by substituting them into equations (2.6.1) and (2.6.4), collecting terms involving like powers of θ, and setting the coefficient of each power of θ to zero.

After using Taylor's series expansion, ignoring higher powers of θ and performing the required integration, we obtain the dimensionless mass flow rate given by

$$V_D=\frac{2\theta_w A_1}{(2\sin\theta_w)^{3/2}} \tag{2.6.8}$$

where

$$A_1^2=\left(\frac{k'+2}{k'-1}\right)\left(\frac{1-\xi_1^{-(k'-1)}}{1-\xi_1^{-(k'+2)}}\right) \left(1+\frac{(9\sin\phi-3)\theta_w^2+(16\sin\phi-8)\theta_w\gamma_w}{6(1+\sin\phi)}\right) \tag{2.6.9}$$

The above solution can be compared with the smooth wall, radial gravity (SWRG) solution and with data. The Brennen–Pearce solution predicts a lower mass flow rate than the SWRG solution. This is to be expected, as the former includes the effect of wall roughness. The predictions of the Brennen–Pearce solution differ from the measured values by 30–50 % of the latter for wall angles in the range 5–40°.The solution overestimates radial velocities considerably, but captures qualitatively the variation of the velocity in the circumferential direction.

The Brennen–Pearce solution represents a significant improvement over the smooth wall, radial gravity solution. Higher order solutions can in principle be constructed by retaining more terms in the expansions. However, this has not been done so far, probably because a coupled system of nonlinear ordinary differential equations is obtained.

2.7 *The Haar–von Karman Hypothesis*

Haar and von Karman (1909) in their paper on three-dimensional stress and deformation fields in static media, considered a special case where two of the principal stresses were equal. This assumption is called the *Haar–von Karman hypothesis*, and is incorporated in the present problem which is stated below.

The principal stresses are given by σ_1, σ_2, and $\sigma_3=\sigma_{\phi'\phi'}$, with σ_1 chosen to be $\geq$ σ_2. Thus there are three possible ways of implementing the hypothesis:

(i) $\sigma_1=\sigma_2$,

(ii) $\sigma_1=\sigma_3=\sigma_{\phi'\phi'}$,

(iii) $\sigma_2=\sigma_3=\sigma_{\phi'\phi'}$.

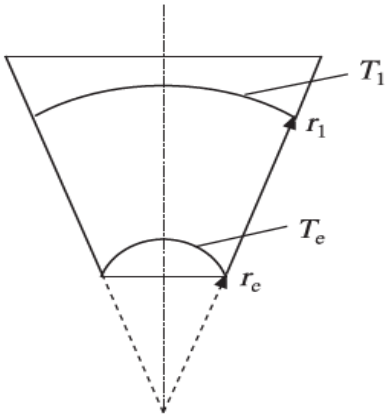

Figure 3: The traction-free surfaces T_1 and T_e. Here T_1 represents the upper free surface of the fill, and r_e is the radial coordinate corresponding to the edge of the exit slot

Case (i) can be ruled out as because for a hopper with rough walls, the shear stress $\sigma_{r\theta}(r, \theta = \theta_w)$ at the wall is nonzero in general. As the σ_1 and σ_2 axes lie in the r-θ plane, a nonzero value of $\sigma_{r\theta}$ implies that $\sigma_1 \neq \sigma_2$.

Moreover at the center-line, the condition of zero shear stress implies that $\sigma_{r\theta} = 0$ and assuming that $\tau \neq 0$, it follows from equation (2.5.8) that $\gamma' = 0$ or $\pi/2$. Thus one of the principal stress axes must be vertical. Further, the other two axes must lie in the horizontal plane, and must be equal on account of symmetry.

Hence at the centerline, Case (ii) corresponds to a passive state of stress, with the σ_1 axis horizontal, and Case (iii) to an active state of stress, with the σ_1 axis vertical. As two of the principal stresses are equal at the centerline, this result provides a justification for the Haar–von Karman hypothesis. At other points ($\theta \neq 0$), the basis for this hypothesis is not clear. Nevertheless. it has been widely used (Savage, 1967; Williams, 1977; Nguyen et al., 1979; Cleaver and Nedderman, 1993b).

The Case (ii) where σ_1 axis is horizontal, this passive state of stress is usually assumed to be appropriate for downward flow through the hopper. However, it appears difficult to rigorously establish this result for the case of three-dimensional hopper flow. Here we shall assume that

$$\sigma_1 = \sigma_3 = \sigma_{\phi'\phi'} \tag{2.7.1}$$

This notion of active and passive states is described in scholarly articles (Rankine, 1857).

3 RTBN - Equation

3.1 *Rose Tanaka Beverloo Nedderman (RTBN) correlation*

When coarse materials flow from hoppers, it is generally agreed that the mass flow rate $\dot{M}$ is approximately independent of the head of material H, provided H is greater than a few multiples of the slot width D (Beverloo, 1961; Nedderman, 1992, p.293).

Assuming that $\dot{M}$ is independent of the head of material, it may be expected to depend on the dimensions of the exit slot, the acceleration due to gravity g, the particle diameter d_p, the density ρ of the granular material, and the frictional properties of the granular and wall materials.

There is a range of particle diameters for which $\dot{M}$ is independent of d_p. For a circular exit slot or orifice of diameter D, we have $\dot{M} = \dot{M}(D, g, \rho)$. As the flow is driven by gravity, the velocity scale can be chosen as $\sqrt{gD}$. Hence $\dot{M}$, which is the product of the density, the average vertical velocity, and the cross-sectional area, is given by

$$\dot{M} \simeq \rho \times \sqrt{gD} \times (\pi D^2/4) \tag{3.1.1}$$

Thus $\dot{M} \propto D^{5/2}$ for a circular orifice.

Based on experiments, it was found that $\dot{M} \propto D^{2.77}$ for sand and $\dot{M} \propto D^{2.95}$ for spinach seeds. Bev-

erloo proposed an equation in 1961,

$$\dot{M} = 0.58\ \rho\sqrt{g}\ (D - k_* d_p)^{5/2} \tag{3.1.2}$$

The deviation of the exponent from the expected value of 2.5 was attributed to the existence of an empty zone adjacent to the edge of the orifice. So the expression was modified into $\dot{M} \propto (D - k_* d_p)^{5/2}$, where d_p is the particle diameter and k_* is a constant. Nedderman recommended that it should be used only for particle diameters in the range $0.4mm < d_p < D/6$, where D is the diameter of the exit slot. Above the upper limit, mechanical interlocking of particles is likely to occur at the exit; below the lower limit, drag caused by the interstitial air may affect the flow rate.

For hoppers with steep walls, this equation underestimates the mass flow rate $\dot{M}$ considerably. The effect of the wall angle θ_w on $\dot{M}$ was examined in another paper (Rose and Tanaka, 1959). Using data obtained from cylindrical bunkers, with θ_w in the range 15^o - 90^o, they found that

$$\dot{M} \propto F(\theta_w, \beta) \tag{3.1.3}$$

where,

$$F(\theta_w, \beta) = \begin{cases} (\frac{\tan\theta_w}{\tan\beta})^{-0.35}, & \text{if } \theta_w \le \beta \\ 1 \qquad\qquad , & \text{if } \theta_w > \beta \end{cases} \tag{3.1.4}$$

here, β is the angle between the vertical and the boundary of the stagnant zone in a bin.

Nedderman (1992, p.296) combined the above with Beverloo's equation to obtain

$$\dot{M} = 0.57\rho\sqrt{g}(D - 1.4d_p)^{5/2} F(\theta_w, \beta) \tag{3.1.5}$$

This equation is also called the Rose-Tanaka-Beverloo-Nedderman (RTBN) correlation.

To compare with data, a dimensionless mass flow rate V_D is introduced, which is defined by,

$$V_D = \dot{M}/(\rho A\sqrt{gD}) \tag{3.1.6}$$

where A and D are the cross sectional area and diameter of the exit slot respectively. Using the equation (3.1.6), the mass flow rate (3.1.5) can be rewritten as,

$$V_D = 0.74F(\theta_w, \beta)G(k_* d_p, D) \tag{3.1.7}$$

where $G = [1 - (k_* d_p/D)]^{5/2}$ for an axisymmetric hopper.

4 SWRG - Equation

4.1 *The smooth wall, radial gravity (SWRG) problem for incompressible flow*

Considering the work of Savage, 1965; Davidson and Nedderman, 1973 we see that

$$\bar{\sigma} \;=\; \frac{1}{1-\sin\phi}\left(\frac{\xi}{2k-1} - \frac{\bar{A}^2}{(k+2)\xi^4}\right) \;+\; c_1\xi^{2k} \tag{4.1.1}$$

where,

$$\bar{\sigma} \equiv \sigma/\left(\rho g r_e\right); \quad \xi \equiv r/r_e; \qquad k \equiv (2\sin\phi)/(1-\sin\phi) \tag{4.1.2}$$

c_1 is an integration constant, and r_e is the radial coordinate corresponding to the hopper exit. The dimension less constant $\bar{A}$ is related to the radial component of velocity v_r by

$$u \equiv v_r/\sqrt{g r_e} = -\bar{A}/\xi^2 \tag{4.1.3}$$

The constants $\bar{A}$ and c_1 can be determined using the traction-free boundary conditions which states - $\xi = \xi_i$ where i is a point on the boundary

$$\overline{A}^2 = \left(\frac{k+2}{2k-1}\right)\left(\frac{1-\xi_1^{-(2k-1)}}{1-\xi_1^{-(2k+4)}}\right) \tag{4.1.4}$$

$$c_1 = -\frac{1}{(1-\sin\phi)(2k-1)}\left(\frac{\xi_1^{-(2k-1)} - \xi_1^{-(2k+4)}}{1-\xi_1^{-(2k+4)}}\right) \tag{4.1.5}$$

where, $\xi_1 = r_1/r_e$, solving the above equations we get;

$$V_D = \frac{8\,(1-\cos\theta_w)}{(2\sin\theta_w)^{5/2}}\overline{A} \tag{4.1.6}$$

For the special case of a deep hopper i.e $\xi_1 >> 1$ the equation simplifies to

$$V_D \approx \frac{8\,(1-\cos\theta_w)}{(2\sin\theta_w)^{5/2}}\left(\frac{k+2}{2k-1}\right)^{1/2}, \quad \xi_1 \gg 1 \tag{4.1.7}$$

5 N - Equation

5.1 *The solution of Nguyen et al. (1979)*

This is an approximate solution that accounts for wall roughness and vertical gravity, using the approach proposed by Brennen and Pearce (1978) for a wedge-shaped hopper.

Omitting terms involving cubes and higher powers of θ, the solution is given by:

$$u = -\frac{\overline{A}}{\xi^2}\left(1 - \frac{3\gamma_w}{\theta_w}\theta^2\right); \quad \nu \equiv \frac{\nu_\theta}{\sqrt{gr_e}} = 0$$
$$\gamma' = \gamma_w\frac{\theta}{\theta_w}; \quad \overline{\sigma} = \overline{\sigma}_o(\xi) + \overline{\sigma}_2(\xi)\frac{\theta}{\theta_w}^2 \tag{5.1.1}$$

where,

$$\overline{A} = \frac{k'+2}{2k'-1}\left(1 + \frac{\theta_w(sin\phi(14\gamma_w + 5\theta_w) - \theta_w)}{2(1+sin\phi)}\right) x\left(\frac{1-\xi_1^{-2k'-1}}{1-\xi_1^{2k'+4}}\right); \tag{5.1.2}$$

$$k = \frac{2\sin\phi}{(1-\sin\phi)}\left(1 + \frac{\gamma_w}{\theta_w}\right); \tag{5.1.3}$$

$$\sigma_0(\xi) = \left(\frac{1}{1-\sin\phi}\right)\left(\frac{\xi}{2k'-1} - \frac{\overline{A}^2}{(k'+2)\xi^4}\right) + c_1\xi^{2k}; \tag{5.1.4}$$

$$\sigma_2(\xi) = \left(\frac{\sin\phi\gamma_w(4\theta_w + 3\gamma_w)}{\cos^2\phi(2k'-1)} + \frac{\theta_w^2}{2(1+\sin\phi)}\right)\xi + \left(\frac{\sin\phi\gamma_w(\theta_w - 3\gamma_w)\overline{A}^2}{\cos^2\phi(k'+2)\xi^4}\right) + \left(\frac{\sin\phi\gamma_w((2k'+3)\theta_w + 3\gamma_w)}{1+\sin\phi}\right)c_1\xi^{2k'}; \tag{5.1.5}$$

$$c_1 = \frac{1}{(1-\sin\phi)(2k'-1)}\Big(1 + \frac{\theta_w}{2(1+\sin\phi)} (\sin\phi(\gamma_w(6-4k') + 5\theta_w) - \theta_w)\Big) \tag{5.1.6}$$

Using the above equations, the dimensionless mass flow rate equation is given by

$$V_D = \frac{8E(\gamma_w, \theta_w)A}{(2\sin\theta_w)^{5/2}} \tag{5.1.7}$$

where,

$$E(\gamma_w, \theta_w) \equiv (1-\cos\theta_w) \times \left(1 - \frac{3\gamma_w}{\theta_w(1-\cos\theta_w)}\right) \big((2\theta_w\sin\theta_w + (2-\theta_w^2)\cos\theta_w - 2)\big) \tag{5.1.8}$$

6 Radial Stress and Velocity Field

6.1 *Experimental observation*

This section majorly deals with the velocity profiles which are estimated through experiments by Cleaver and Nedderman (1993a) using a tracer technique.

Experimental setup: They used a tracer technique in a hopper fitted with a guide tube. A ceramic tracer particle which was larger than the particle, was introduced into the hopper through the guide tube. Then they measured tracer's residence time(Tr) which is the time that the tracer took to reach the hopper exit.

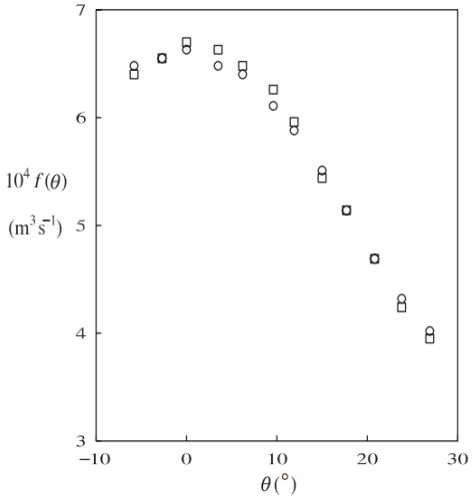

Figure 4: Experimental & observed variation of $f(\theta)$ vs $\theta(^\circ)$

Velocity profile: Spherical coordinate system with the hopper's apparent vertex was taken as the origin and assumed to be radial and incompressible flow and the radial component of velocity (v_r) can be expressed as equation 6.1.1.

$$v_r = -\frac{f(\theta)}{r^2} \tag{6.1.1}$$

By measuring T_r and plotting it against R_0^3, function $f(\theta)$ was determined in equation 6.1.2.

$$T_r = \frac{R_0^3 - Re^3}{3f(\theta)} \tag{6.1.2}$$

The data shows that the magnitude of the radial velocity decreases as θ increases because of the retarding effect of wall friction, except near the center-line (Figure 4). This reflects the retarding effect of wall friction.

In a radial and incompressible flow, $f(\theta)$ should turn out to be proportional to the mass flow rate and this consistency was observed in the data.

Data: The data was taken for the two orifice diameters. The data for the smaller orifice was scaled by the ratio of mass flow rates of the larger to the smaller orifice.

6.2 *The Radial Stress and Velocity Fields for the Mohr–Coulomb Yield Condition and the Haar–von Karman Hypothesis*

Finding Radial Stresses :

The Haar–von Karman hypothesis can be applied to the hopper problem :

$$\sigma_3 = \sigma_{\phi'\phi'} = \sigma_1 \geq \sigma_2 \tag{6.2.1}$$

Using the Mohr–Coulomb yield condition :

$$\tau = \sigma sin\phi \tag{6.2.2}$$

The stress components are given by :

$$\begin{aligned} \boldsymbol{\sigma}_{rr} &= \sigma(1 - sin\phi\ cos2\gamma') \\ \boldsymbol{\sigma}_{\theta\theta} &= \sigma(1 + sin\phi\ cos2\gamma') \\ \boldsymbol{\sigma}_{r\theta} &= -\sigma sin\phi\ sin2\gamma' \\ \boldsymbol{\sigma}_{\phi'\phi'} &= \sigma_1 = \sigma(1 + sin\phi) \end{aligned} \tag{6.2.3}$$

In above equations , σ is the mean stress in the r-θ plane. And the interpretations of σ_1, σ_2 & γ can be obtained from the figure 5.

Finding Velocity Field :

From the mass balance equation (2.5.3) assuming that the flow is radial and incompressible we obtain the equation 6.2.4 as a result

$$\nu_r = -f(\theta)/r^2; \quad \nu_\theta = 0; \quad \nu'_\phi = 0 \tag{6.2.4}$$

Where $f(\theta)$ is given by

$$f(\theta) = f(0)\ exp\Big(-3\int_0^\theta tan(2g_*(\omega))d\omega \Big) \tag{6.2.5}$$

Overall velocity field is derived using mass balance eqaution (2.5.3) and inertial momentum balance equations (2.6.2, 2.6.3). As in the case of plane flow (section 2.4), the inertia-free momentum balances admit a particular solution of the form (Cleaver and Nedderman, 1993b)

$$\sigma_* = \sigma/(\rho g r_e) = b_*(\theta)\xi\ ; \quad \gamma' = g_*(\theta) \tag{6.2.6}$$

where $\rho = \rho_p \nu$ is the particle density, g is the acceleration due to gravity, r_e is the radial coordinate corresponding to the edge of the exit slot (Figure 5), and $\xi = r/r_e$.

The functions $b_*(\theta)$ and $g_*(\theta)$ are determined by integrating the following differential equations, which are obtained by substituting (equation 6.2.6) into the inertia-free momentum balances

$$\begin{aligned} &\frac{d}{d\theta}(b_* sin\ \phi\ sin2g_*) = \\ &b_*[1 - sin\phi(4cos2g_*\ +\ sin2g_* cot\theta + 1)] + cos\theta \end{aligned} \tag{6.2.7}$$

$$\begin{aligned} &\frac{d}{d\theta}[b_*(1 + sin\ \phi_*\ cos2g_*)] = \\ &\qquad b_* sin\phi[4sin2g_*\ +\ cot\theta(1 - cos2g_*)] \end{aligned} \tag{6.2.8}$$

For a passive solution, the boundary conditions are given by

$$g_*(0) = 0; g_*(\theta_w) = \gamma_w \tag{6.2.9}$$

An interesting implication of equation 6.2.6 is that It is instructive to consider the initial value problem defined by equations(6.2.7) & (6.2.8) and the initial conditions

$$g_*(0) = 0\ ; \quad b_*(0) = b_{*0} \tag{6.2.10}$$

7 Results & Conclusions

7.1 *Comparing RTBN, SWRG & N equations*

In this section, we provide a comparison of measured and predicted mass flow rates solved using the Haar-von Kármán Hypothesis.

In Figure 6, the curves are labeled as SWRG, RTBN, and N, which depict the V_D (Dimensionless mass flow rate, defined by Eq. 7.1.1) values obtained

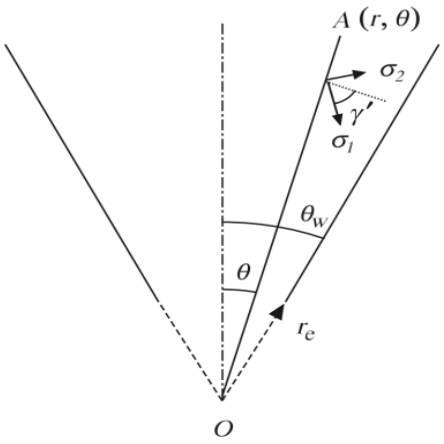

Figure 5: σ_1 & σ_2 are the major and minor principal stresses respectively in the r-θ plane, and γ' is the angle measured anticlockwise from σ_1 axis to the circumferential direction

using the SWRG analysis, Rose-Tanaka-Beverloo-Nedderman correlation, and the Nguyen analysis, respectively.

$$V_D \equiv \frac{\dot{M}}{\rho_p \nu A \sqrt{g} D} \tag{7.1.1}$$

We have calculated the parameters for the data of Nguyen, represented by squares. We notice that the SWRG analysis overestimates the mass flow rates quite a bit, with errors ranging from 60% to 3% for wall angles between 10°and 35 °.

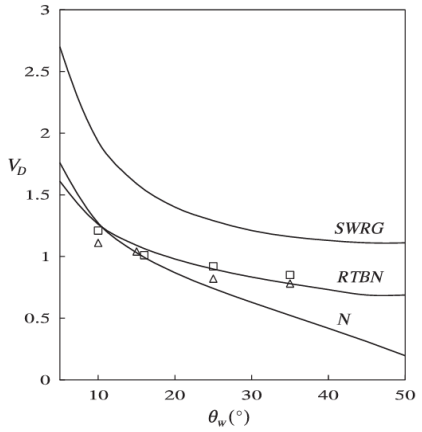

Figure 6: Comparative interpretations among the three equations

While Nguyen's analysis performs better with only a 5% error at a wall angle of 10 °, but the error increases to 38% at 35 °. So from this, we can say Nguyen's method might not be accurate for larger wall angles since it does not consider higher powers of the angle.

But when we analyze the RTBN correlation, we see that it performs well with estimates within 2% to 8% of the measured values. On the other hand, the Beverloo correlation underestimates the mass flow rate, especially at the small angles.

There is data from Zeininger and Brennen (1985) as well, which is represented by triangles, and it also aligns well with the RTBN correlation. But due to some necessary data missing from Zeininger and Brennen's data, we were unable to compare this data with the predictions of the SWRG model or Nguyen's model.

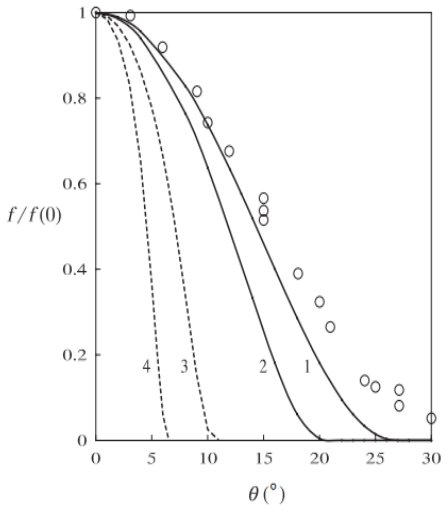

Figure 7: Profiles of the dimensionless radial velocity for granular flow in a conical hopper

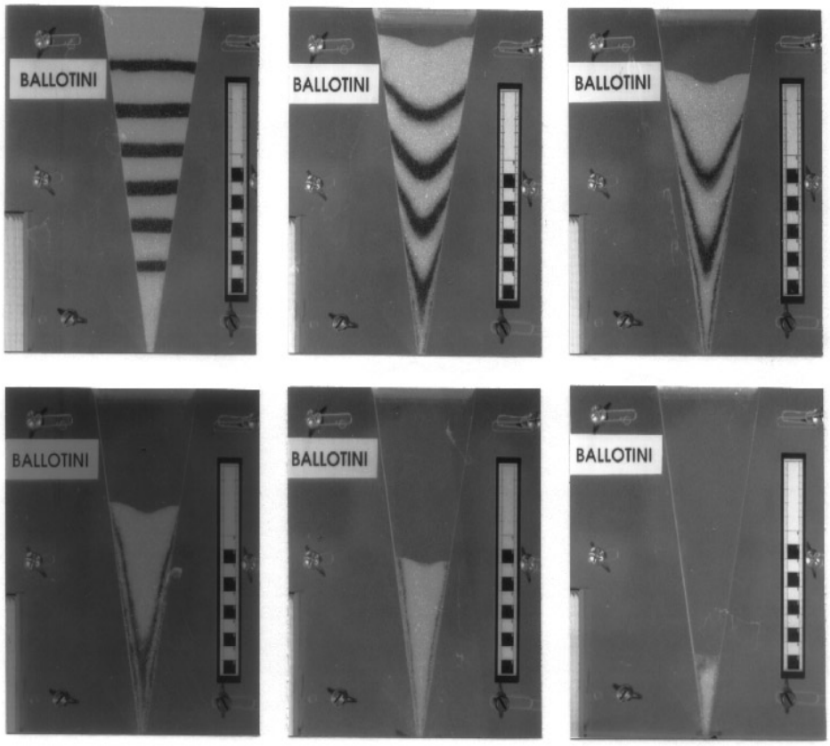

Figure 8: Plug-flow patterns within undisturbed conical hoppers. Scale in cm.

7.2 *Comparison of Predicted and Measured Velocity Profiles*

Here we compare predicted velocity profiles with the measurements of Cleaver and Nedderman (1993a) for the flow of polypropylene granules through a hopper lined with sandpaper.

The angle of internal friction ϕ and the angle of wall friction δ were determined using an annular shear cell. Three tests were conducted to determine ϕ, and the minimum value ϕ_{min} and the maximum value ϕ_{max} were reported for each test. The mean values of ϕ_{min} and ϕ_{max} were 30.4°and 37.1°, respectively. The mean value of δ was 28.5°.

To make a proper comparison, we use an alternative approach described by Cleaver and Nedderman (1993b), which makes use of the Drucker-Prager Yield condition and Levy's flow rule. As shown in Fig.7, the results given by Mohr–Coulomb yield condition and the Haar–von Karman hypothesis are worse than the proposed alternative approach. It is to be noted that this conclusion is also applicable to their experiments with other granular materials (spherical kale seeds, glass beads, etc).

8 Annexure

8.1 *Important Notations*

d_p - particle diameter
det - determinant of a tensor or matrix
$\boldsymbol{n}$ - unit vector normal to a bounding surface
r - radial coordinate
$\boldsymbol{t_n}$ - stress vector in the direction of $\boldsymbol{n}$
tr - sum of the diagonal components of a tensor or matrix
C - rate of compression in the direction of $\boldsymbol{n}$
D - width of the exit slot
H - head of the granular material
$\dot{M}$ - mass flow rate
N - normal stress
S - rate of shear in the direction of unit vector $\boldsymbol{t}$
T - shear stress
V_D - dimensionless mass flow rate
β - filling angle
γ - orientation of the major principal axis
δ - angle of wall friction
θ - circumferential coordinate
θ_w - wall angle of the hopper
ν - solid fraction

ξ - dimensionless radial coordinate
ϕ or ϕ_* - angle of internal friction
ϕ' - spherical coordinate

8.2 *Model Studies*

A physical two-dimensional model was created by A A Mills (1996) to study and validate the equations regarding mass flow rate and velocity profile of granular flow in a conical hopper. The wall angle was taken to be 14^o, and the walls were polished with anti-static fluid to eliminate electrostatic adhesion. The patterns shown in this system at different times are referenced in Fig.8.

It is to be noted that the 2-D model accurately reflects the behaviour of the corresponding 3-D model. This is because the sequence of emptying periods obtained when all models were set to the same width of aperture, and loaded with the same mass of ballotini, was the same as that observed with the 3-D glass vessels (A A Mills, 1996).

8.3 *Future Work*

The approach we would like to apply in this specific problem (granular flow in hourglass), would be to describe the shape of an hourglass mathematically using machine learning regression models. This would decrease the computational time, and give us a basis to construct the boundaries of our system.

Next, we would take the approach proposed by Brennen and Pearce (1978), which is to solve the balance equations and constitutive relations while considering for wall roughness and vertical gravity. We would expand the equation using Taylor or Laurent series, and use other statistic models to elegantly represent the equation by integrating the modified version of the Hypoplastic-viscous model proposed by Eibl and Rombach (1988).

9 References

A A Mills (1996) | Mechanics of the sandglass, published in *Eur. J. Phys. 17.*

Beverloo (1961) | The flow of granular solids through orifices, published in *Chem. Eng. Sci. 15.*

Brennen and Pearce (1978) | Granular material flow in two-dimensional hoppers, published in *Trans. ASME E J. Appl. Mech. 45.*

Cleaver and Nedderman (1993a) | Measurement of velocity profiles in conical hoppers, published in *Chem. Eng. Sci. 48.*

Cleaver and Nedderman (1993b) | Theoretical prediction of stress and velocity profiles in conical hoppers, published in *Chem. Eng. Sci. 48.*

Davidson and Nedderman (1973) | The hourglass theory of hopper flow. Trans. Inst, published in *Chem. Eng. 51.*

Eibl and Rombach (1988) | Numerical investigations on discharging silos, published in *Numerical Methods in Geomechanics*, G. Swoboda, ed. (Balkema, Rotterdam).

Haar and von Karman (1909) | Zur theorie der spannungszustaende in plastischen und sandartigen medien (On the theory of tensile states in plastic and sand-like media), published in *Nachr. Ges. Wiss. Goettingen Math. Phys. Klasse 2.*

Hosseini-Ashrafi and Tuzun (1993) | A tomographic study of voidage profiles in axially symmetric granular flow, published in *Chem. Eng. Sci. 48.*

Hunter (1983) | Mechanics of Continuous Media (Ellis Horwood, Chichester), published in *Journal of Applied Mathematics and Mechanics.*

Nedderman (1992) | Statics and Kinematics of Granular Materials (Cambridge University Press, Cambridge), published in *J. Fluid Mech. vol.286.*

Nguyen (1979) | Gravity flow of granular materials in conical hoppers, published in *Trans. ASME E J. Appl. Mech. 46.*

Rankine (1857) | On the stability of loose earth, published in *Phil. Trans. R. Soc. 147.*

Rose and Tanaka (1959) | Rate of discharge of granular materials from bins and hoppers, published in *The Engineer (Lond.) 208.*

Savage (1965) | The mass flow of granular material from coupled velocity-stress fields, published in *Brit. J. Appl. Phys. 16.*

Savage (1967) | Gravity flow of a cohesionless bulk solid in a converging conical channel, published in *Int. J. Mech. Sci. 9.*

Sokolovskii (1965) | Statics of Granular Media. (Pergamon, Oxford).

Williams (1977) | The rate of discharge of coarse granular materials from conical mass flow hoppers, published in *Chem. Eng. Sci. 32.*

Zeininger and Brennen (1985) | Intersitial fluid effects in hopper flows of granular material, published in *In Cavitation and Multiphase Flow Forum – 1985.* (American Society of Mechanical Engineers, New York).